Answers to the Questions of the FAIR ECE regarding the Update to the Technical Design Report for the $\overline{\text{P}}$ANDA Electromagnetic Calorimeter

The $\overline{\text{P}}$ANDA Collaboration

29th March 2021

1 Cost and Schedule

1.1 Crystal Funding

Question:
The current EMCAL schedule relies on Russian funding to acquire the additional PWO crystals needed for the barrel calorimeter and increasing the production rate at Crytur in order to meet your current schedule. As there is an inherent risk associated with this, please provide an alternative plan to meet the current project schedule in case the Russian funding does not become available, or describe the impact of not obtaining this funding on the current schedule.

Answer:
Due to the funding-driven staged approach of civil construction and the delays accumulated in connection with Covid-19, the current FAIR schedule calls for the completion of the electromagnetic calorimeter in 2025. In the update report the previously planned completion year 2023 was given. Therefore, Russian funding is not needed until the end of 2022. In the meantime, we are raising money from various sources to complete the first 3 slices. If the Russian funding is severely delayed, we will try to complete at least 50 % of the barrel calorimeter. Depending on the flow of funds, the crystals can be ordered from Crytur at any time. Ultimately, we expect full funding from Russia, as Russia has already invested heavily in FAIR and $\overline{\text{P}}$ANDA.

1.2 Single Vendor

Question:
With only one vendor Crytur to produce the additional PWO crystals for the barrel, please describe how you plan to control the cost and delivery schedule for the remaining crystals, both for the 12/16 slices that are planned to be completed by 2023, as well as all 16 slices. In the case of a cost increase due to the investment in additional ovens at Crytur, please provide an evaluation of other possible alternatives to obtain the additional needed crystals, such as the possibility to procure additional crystals from the alternative vendor SICCAS, using previously rejected spare crystals, and/or repurposing of other radiator material, and what impact this would have on the cost and schedule.

Answer:
As of now, no producer for PWO crystals in a satisfactory quality other than Crytur (Czech Republic) could be identified. Several prototyping campaigns for crystals have been performed together with different companies, including SICCAS (China) until 2012, which utilizes the Bridgeman technology for growing crystals in contrast to the Czochralski method used by BTCP (Russia) and Crytur. The conclusion from the analysis of the samples obtained from SICCAS was, that the Bridgeman technology does not allow for an as precise control of the doping distributions (lanthanum and yttrium) as would be required in order to constrain the crystal parameters, such as transmittance at different spectral wavelengths, radiation-induced transmittance change (dk value) and light yield within the technically required range. From the experience of a small series production of $\overline{\text{P}}$ANDA crystals produced by SICCAS until 2012, one would estimate the number of quality-rejected crystals to be inacceptably high. Unfortunately, SICCAS showed minor interest in later inquiries about evaluation of samples for the $\overline{\text{P}}$ANDA project after 2012. With Crytur as the currently only vendor continuously producing crystals, the EMC time schedule foresees a staged production of crystals effectively from the milestone ME1 (funding established) in Q4/2022 until the completion of the twelfth slice segment in 2025 with the consecutive assembly of all crystal-complete segments inbetween. There is currently no alternative plan for obtaining the required crystals otherwise. However, a moderate number of formerly rejected SICCAS and BTCP crystals could be reincorporated by relaxing the upper acceptance limit for dk from 1.1 to $1.2\,\mathrm{m}^{-1}$. Those crystals will still remain inside the allowed operation conditions wrt. radiation tolerance and light yield if mounted in the most backward part of the barrel EMC. Apart from this, the raw material needed to produce the remaining ≈ 6200 crystals was purchased several years ago and therefore has no impact on potential further cost and schedule shifts.

1.3 Performance Impact of Partial Barrel

Question:
In the case that only up to $\approx 75\,\%$ of the barrel is instrumented on Day 1, please describe the impact this would have on the detector performance and physics capabilities and if

there are ways to recover this performance.

Answer:
In order to quantify the impact of the DAY-1-setup on the efficiency and background suppression performance of the software trigger, the reconstruction of five physics channels has been carried out. These were selected to cover different fields of physics and different orders-of-magnitude of the corresponding cross-section. Among those five channels, three comprise electrons, positrons and/or photons and are thus directly affected by the reduced EMC setup. It has been (effectively) simulated by two times worse cluster energy resolution (to simulate the effect of a preliminary calibration for the software trigger) as well as a 25 % reduction of the EMC crystal slices symmetrically at the top and bottom part of the detector barrel.

The channel with both electrons and neutrals in the final states is $\bar{p}p \to e^+e^-\pi^0 \to e^+e^-\gamma\gamma$ (C1), while the other two without photons are $\bar{p}p \to e^+e^-$ (C2) and $\bar{p}p \to J/\psi(\to e^+e^-)\pi^+\pi^-$ (C3).

In order to identify the signal and significantly suppress background for the purpose of event selection, only the rather simple requirement $E/p > 0.7$ to the electron and positron candidates was applied, with p being the reconstructed track momentum, and E being the reconstructed energy of the electro-magnetic cluster. The effect of the DAY-1-setup is on the one hand the reduced resolution of E/p, on the other hand the missing of this measurement in the spatial regions of missing crystals.

The impact on channels C2 and C3 was a reduction of the event reconstruction efficiency by about 22 % to 24 %. In case of C1, the additional efficiency loss of the reconstructed π^0 meson together with the worse particle identification resulted in an event selection efficiency loss of about 54%. However, only minor impact was observed for the other two (non electron and photon) channels $\bar{p}p \to J/\psi(\to \mu^+\mu^-)\pi^+\pi^-$ and $\bar{p}p \to \Lambda\bar{\Lambda}$.

Therefore the DAY-1-setup does not severely affect the planned early measurements in the field of hyperon physics, and, combining both leptonic decay channels of the J/ψ with almost identical branching fractions, even charmonium spectroscopy like energy scan measurements of narrow resonances like the $X(3872)$ might only have a rather negligible relative effciency reduction of about 10 % to 12 % (= 22 % loss in only 50 % of the events). This effectively means a somewhat longer measurement time.

The physics programme of other channels with higher multiplicity and which require full accepance for partial wave analysis have to be delayed until the full barrel is equipped.

1.4 Upgrade Path to Full Barrel

Question:
Please provide clarification on the upgrade path to complete 100 % barrel coverage and describe what impact this would have on the overall $\overline{\text{P}}$ANDA running schedule, including the need to recalibrate the calorimeter system in order to achieve the final overall physics performance.

Answer:
Current planning calls for the completion of 12 of the 16 slices of the barrel calorimeter for the DAY-1-setup. After several beam times of 6 month each year $\overline{\text{P}}$ANDA will have a longer shutdown of 1.5 years for the installation of detector systems like the MVD pixels, forward tracking planes and the forward DISC DIRC. We will make use of that maintenance break to install the remaining slices to minimize the impact on the overall $\overline{\text{P}}$ANDA running schedule.

Recalibration of the calorimeter system can be accomplished within a few days using the π^0 calibration method. By then, we will have plenty of experience. During the beam tests of the forward endcap EMC in Jülich, we will study everything to get a good control of the monitoring and calibration. Experiences will be gained with the backward endcap at MAMI too.

2 Crystal Quality and Performance

2.1 Differences in dk Values

Question:
The dk value of the Crytur PWO crystals after 30 Gy, shown in Fig. 2.15 of TDR update, seems significantly larger that the BTCP PWO-II crystals after 50 Gy, shown in Fig. 4.35 of the 2008 TDR. Please explain the nature of this difference and if there are any ways envisioned that this could be improved for the Crytur crystals.

Answer:
Fig. 4.35 of the original TDR reflects the results obtained with crystals from the preproduction run. The tests were performed at BTCP. The comparison of the induced absorption measurements for the total amount of the crystals shipped by BTCP is shown in Fig. 2.3 in the TDR update. A shift of the distribution maximum of $\approx 20\,\%$ was obtained. Most of the crystals produced at Crytur pass the irradiation test in Gießen. So, to compare the distributions in Fig. 2.15 and Fig. 4.35 of the 2008 TDR the corrected maximum at the latter plot should appear at 0.65. In this case, the distributions will practically coincide.

One has to keep in mind two other moments when comparing this data:
Crystals of the pre-production lot at BTCP were cut from ingots produced by using a new batch of raw materials. During the mass production, the rest of the material from the ingots was re-used by melting it together with a new part of the raw material. This recrystallization reduces the overall material requirements and thus allowed us to use the raw material more efficiently and lower the price. It was established experimentally that the average dk value is lower for the first crystallization cycles. dk increases — but stays within $\overline{\text{P}}$ANDA specifications — for five to six recrystallization cycles, but can increase drastically for further cycles. So, crystals for the pre-production lot were cut from ingots grown in early crystallizations. For mass production lots ingots with up to 10 crystallization cycles were used. This can explain the difference in the average dk

values for the pre-production and the mass production lots.

The data presented in Fig. 2.15 of TDR update was obtained at the radiation facility in Gießen. The dose rate was calibrated, and time needed to reach 30 Gy was correctly estimated. Based on the experience with the radiation facility at Gießen during 2008 – 2020 one can conclude that dose rate differences of 2 to 3 times due to the aging of the ^{60}Co source ($T_{\frac{1}{2}} = 5.2714\,\mathrm{a}$) can lead to a dk value difference at the level of 10 % to 20 % depending on the crystal quality. For this reason, it was decided to extend the specification limit from $1.0\,\mathrm{m}^{-1}$ to $1.1\,\mathrm{m}^{-1}$ for data obtained at Gießen. The decision was a compromise covering possible experimental errors and differences of the irradiation processes.

2.2 Hadronic Radiation Damage in PWO

Question:
It is known that hadrons can also cause radiation damage in PWO crystals beyond just ionization. Please provide the expected hadron fluence, including charged and neutral hadrons, and its effect on the performance of the crystals in the barrel and endcap calorimeters.

Answer:
The effect of hadrons on the optical transmission and the detector performance was studied by the CMS Collaboration at CERN [1]. It was shown that the induced damage on the optical transmission is linear in the range $10^{12}\,\mathrm{cm}^{-2}$ to $10^{14}\,\mathrm{cm}^{-2}$ during the irradiation with high energy protons. For example, the induced absorption coefficient dk depends on the fluence F of 24 GeV protons as follows:

$dk\ [\mathrm{m}^{-1}] = 1.492 \times 10^{-13} \times F\ [\mathrm{cm}^{-2}] \pm 4 \times 10^{-14} \times F\ [\mathrm{cm}^{-2}]$

The highest expected fluence in the endcaps in the vicinity of the beam line is $10^{12}\,\mathrm{cm}^{-2}$ over the lifetime of $\overline{\mathrm{P}}$ANDA. It is significantly larger than the fluence in the barrel. Thus, it is expected that induced absorption due to hadron irradiation would be at a level of $0.15\,\mathrm{m}^{-1}$. Is is worth to note, that this is about seven times less than the specification level.

Source:

[1] T. Adams et al. Beam test evaluation of electromagnetic calorimeter modules made from proton-damaged PbWO crystals. *JINST* ***11*** *P04012*, 2016. https://doi.org/10.1088/1748-0221/11/04/P04012

2.3 dk Variations

Question:
From Fig. 2.15, the measured ionization induced absorption coefficient at 420 nm (dk) is in the range from $\sim 0.4\,\mathrm{m}^{-1}$ to $1.1\,\mathrm{m}^{-1}$ for accepted PWO crystals after 30 Gy at room temperature, which according to Fig. 2.16 corresponds to 35 % to 70 % light output loss at −25 °C. Given this range of variability, as well as the variation in the radiation dose

across the detector, what is the effect of these variations over the entire ensemble of crystals in the barrel and endcaps?

Answer:
In Chap. "3.2.2.3 Radiation Hardness" and Table 3.1 of the 2008 TDR the maximum annual dose rate for the backward endcap and barrel crystals was given as 10 Gy. It is lower by more than one order of magnitude than the same dose for the forward endcap EMC. Therefore, while considering an application of the stimulated recovery the radiation hardness is not a crucial parameter for those parts of the EMC. For the forward endcap, the crystal positions are assigned according to the radiation hardness results. Crystals of "better" quality are placed closer to the beamline where the expected radiation dose is higher, as explained in Sec. 3.2.4 of the TDR update. All VPTT submodules have already been built, this issue was already taken into consideration and has been addressed.

2.4 Energy Resolution

Question:
The original TDR states that the energy resolution requirement for the EMCAL is to have a stochastic term $< 2\,\%/\sqrt{E}$ and a constant term $< 1\,\%$. The energy resolution was measured in several prototypes which gave $2.46\,\%/\sqrt{E} \oplus 0.16\,\%/E \oplus 2.32\,\%$ for the PROTO120 barrel prototype and $2.41\,\%/\sqrt{E} \oplus 0.86\,\%$ for the forward endcap prototype, which are both slightly worse than the desired resolution requirement, and it is likely more difficult to achieve the desired resolution in the final full size detectors, especially given the added complication of radiation damage and recovery.

While the prospect of applying optical bleaching using a blue LED described in Section 2.5 would seem to provide a way to speed up recovery while the detector is at its $-25\,^{\circ}\mathrm{C}$ operating temperature, it seems that this would only be possible during short beam off periods, and that the main recovery process would take place only during the long 6 month shutdowns when the detector is warmed back up to room temperature. It is understood that the calibration and monitoring system is designed to achieve and maintain the desired energy resolution, but please provide further details as to how it will do this given the expected levels of ionizing radiation and hadron damage, its variability across the various parts of the detector, the control of thermal variations in the crystals and APDs, and the planned optical bleaching and thermal annealing procedures.

Answer:
In the forward endcap several advancements of the design with respect to an improvement of the energy resolution in the low and medium energy range were derived from the prototype beam time results. These improvents comprise solid couplings of photo detectors and crystals and improvements in the read out electronics. In the forward endcap prototype the couplings needed to be realized in a reversible way in order to allow a reuse of all the cystals involved. In the final design the mounting of photo sensors is

done in a non-reversible process by means of a silicon coupling compound (Dowsil 3145 RTV) resulting in constant and well defined couplings. Modifications in the electronic read out chain comprise the optimization of the APD gain with respect to a balance of signal to noise performance and sensitivity to changes in temperature and high voltage. The corresponding neccessary gains of both the APDs and the APD/VPTT preamplifiers for optimal gain coverage of the dynamic range could only be derived from the data taken in the prototype beam times and the input shaper stages on the SADC boards optimized accordingly. Tests of finished forward endcap submodules with cosmic muons consistently reveal an upper single crystal dynamic range limit of $\gtrsim 12\,\mathrm{GeV}$.

For the barrel the same improvements due to gluing of the APDs to the crystals hold. To improve the signal to noise ratio, an optimization of the APD operation gain is currently beeing studied. It was found that the energy resolution improves up to an APD gain of 500, especially for the lowest photon energies. Using the largest available dynamic range of the APFEL ASIC such a high gain could be applied to regions with $\theta > 60°$ for undamaged crystals at the highest beam momentum.

Concerning the light losses due to the radiation damages, it was established experimentally [1] that the illumination of a PWO crystal with blue light allows to reach full recovery of the radiation damage in a few hours even at $-25\,°\mathrm{C}$. Therefore, it seems possible to perform short sessions of stimulated recovery during breaks in the accelerator operation without warming up the calorimeter. And as it is mentioned in the answer to question 2.3 the most crucial area of the calorimeter is the inner part of forward endcap. For all parts of the $\overline{\mathrm{P}}$ANDA EMC the hadronic part of the radiation field will not cause damage to the structure of the PWO crystals. The experience of the CMS experiment is different, but they use much higher energies. In addition, an optical degradation can be recovered in the same way for the electromagnetic part of the radiation field in case of $\overline{\mathrm{P}}$ANDA. The operation conditions of the stimulated recovery for the detector units will be defined in the nearest future.

A further way to reduce the effect of radiation damage is to increase the gain of the photodetectors.

Source:

[1] R. W. Novotny et al. The PANDA Electromagnetic Calorimeter – A High-Resolution Detector Based on PWO-II. *IEEE Trans. Nucl. Sci.*, 2010. https://doi.org/10.1109/TNS.2009.2033913

3 Photosensors, Electronics and Readout

3.1 APD Irradiation and Annealing Effects

Question:
Section 3.1.2.3 describes irradiation and annealing of the APDs but it is unclear what the conclusions are from these studies. Please summarize what the effects of irradiation to 37 Gy and subsequent annealing has on the APDs.

Answer:
The irradiation and subsequent annealing procedure is a check of the functionality of every single APD under radiation doses corresponding to an estimated full $\overline{\text{P}}$ANDA lifetime dose of 37 Gy in the most forward region of the FWEC with APD-equipped crystals. Not a single failure within the bulk of mass screened APDs (more than 17 000 pieces up to now) in terms of malfunction or significant dark current increase has been observed so far nor has it been expected. Single APDs have been irradiated with orders of manitude higher doses and dose rates during beam tests without noticeable damage to the devices. However, the comparison of the characteristic curves (gain vs. bias voltage) before and after irradiation would reveal insufficient radiation tolerance of a single APD after the screening procedure. The screening is a measure to ensure that all APDs mounted to the calorimeter proved to be operational under irradiation levels to be expected in the experiment.

3.2 Nuclear Counter Effect

Question:
Please provide details on the expected nuclear counter effect in the large area APDs used in the barrel due to EM showers, charged hadrons and neutrons, and corresponding mitigation measures.

Answer:
Nuclear Counter Effect signals in the APDs are measured to occur in the low MeV range. This corresponds to the CMS results when the differences in crystal light yield, APD size and gain, and crystal rear face coverage are taken into account. As all calorimeter crystals read out with APDs are equipped with two photo detectors and, unlike the CMS ECAL, with completely seperated readout each, there is the possibility to identify nuclear counter effects by comparing the signals of these two APDs. In case of significantly differing signal heights of the two APD read out channels belonging to the same crystal the one with the higher output level will be considered as suffering from a nuclear counter effect event. In this case rather than averaging the two signals in the feature extraction, the larger of the two signals would be rejected and only the lower one considered. While the statistical noise in this case, i. e. not considering the averaged signal of both APDs in a nuclear upset, would increase by a factor of $\sqrt{2}$ the calorimeter channel output signal is not lost.

3.3 Preamplifier Protection

Question:
In addition to the nuclear counter effect, EM showers and hadronic interactions can potentially inject large amounts of charge into the front end charge sensitive preamplifier resulting in damage to the CSA. What precautions are there to mitigate this?

Answer for the Forward Endcap:

In the discrete component charge sensitive preamplifiers of the forward endcap the JFET input stage is protected by two diodes, one connected to ground and the other to the positive supply rail. While this protection was implemented to protect the open FET input from accidental electrostatic discharges during handling, the diodes will equally well protect the preamp from excessive electrical charges of other origins.

Answer for the Barrel and Backward Endcap:
There is a set of events which might cause injection of large amounts of charge into the amplifier input e. g. electrostatic discharges (ESD) during assembly and handling of the electronics. Also fast ramping of the high voltage leads to an injection of charge into the input gate due to the coupling capacitor.

In case of the ASIC front-end for the barrel and the backward endcap the inputs of the APFEL ASIC are protected by ESD protection structures. These structures contains large area diodes which divert the over voltage caused by the charge injection to the power supply.

3.4 MTBF of SADCs

Question:
In Section 4.3.1.7 it is mentioned that the MTBF for the combined system of FPGAs and SADCs is $\sim 17\,\text{min}$. What is the recovery procedure and what is the impact on the live time?

Answer:
A class of SEU damages to the configuration memory, which are not automatically repaired within the device requires a partial or a full reconfiguration of the effected FPGA. The full reconfiguration and startup procedure lasts for approximately 200 ms.

Although the final firmware of the SADC is not yet ready, the proposed SEU recovery can proceed in the following way:

Irreparable SEU events detected by the SEM will be announced by the SADC by sending a failure message via the optical link to the DAQ. The message will contain a time stamp of the SEU occurrence. From this moment on until the next message containing the recovery time stamp, the device will be considered as not contributing to the data stream. The device will also send a signal via an electrical link to a Crate Controller, which in turn will initiate the reconfiguration of the device. The Crate Controller will also repeat the failure message to the global control system via its own optical link.

3.5 γ Irradiation of SADCs

Question:
There is also a short discussion on proton and neutron irradiation studies for the SADC, but were any studies done using ionizing radiation, e. g. γ from ^{60}Co?

Answer:

"The photon fluence rate is comparable to that of neutrons, and could therefore pose a risk. For a photon to cause an SEU, however, a photonuclear reaction in the device is required. The cross sections for photonuclear reactions are generally much smaller than nuclear reactions caused by protons or neutrons, as the interaction is purely electromagnetic. For this reason, neither photons are expected to be a concern with respect to SEUs in the FPGA, and the expected SEU rate has been determined only for neutron-induced upsets."
Cited from: M. Preston et al., "Proton- and Neutron-Induced Single-Event Upsets in FPGAs for the PANDA Experiment," in IEEE Transactions on Nuclear Science, vol. 67, no. 6, pp. 1093–1106, June 2020, doi: 10.1109/TNS.2020.2987173.

3.6 Long-term Stability of SADCs

Question:
Section 4.3.1.8 describes the post-production testing of the SADCs but does not mention any long term stability testing. Are any such tests being done as part of the acceptance and QA procedure?

Answer:
A number of prototypes and at least 15 SADC modules from the volume production were extensively tested in KVI (Groningen), RUB (Bochum), JLU (Gießen), JGU (Mainz), including long-term power endurance. No failures were reported so far. Long term stability testing of the SADCs for the forward endcap will be performed before the beam tests at Jülich.

3.7 Gain Increase vs. Light Loss

Question:
It is anticipated that it will be necessary to increase the gains of both the APDs and the VPTTs due to loss of light in the crystals resulting from radiation damage. The system to adjust the gains is described, but can you provide information on whether the available range of gain adjustment will be sufficient to compensate for the expected light loss. Also, increasing the gain in the APDs will also increase the noise. What effect will this have on the performance?

Answer for the Forward Endcap:
While crystals in the innermost region of the forward endcap have been choosen to be the most radiation hard ones available the expected light loss without annealing may still result in up to 30 % light yield loss in single crystals. The VPTT and corresponding preamp gains in the beginning are chosen to result in equal responses within groups of four neighboring readout channels that are supplied by one common high voltage channel. The primary operating voltage of the VPTTs lies in a range of 750 V to 1000 V at the begin of the experiment. The operational limit of the VPTT devices and the corresponding voltage divider circuit is 1500 V. Operating at this limit the gain of the

VPTTs increases by at least 50 % thus allowing to cover up even the highest expectable light yield losses of the crystals. In case of the APDs in the forward endcap that are operated at voltages corresponding to a gain of 200 a change in gain by up to 50 % — not that such an increase of gain is expected to be necessary in the APD equipped region of the forward endcap — would result in still lower gain operation conditions compared to the calorimeter barrel on the first day of operation and therefore considered safe and easy to realize.

Answer for the Barrel:
The calorimeter will be equipped with blue high-intensity annealing LEDs for damage recovery to avoid radiation damage accumulation. Thus only a moderate gain increase of up to 30 % is needed. Each APD gain can be individually adjusted in a sufficient range, for example with respect to its θ position and the light yield loss of the corresponding crystal.

Nevertheless, independent from the radiation damage management, the study of the impact of an increased APD gain has been performed. By using a close-to-final front-end version for the barrel and backward endcap part, including the foreseen power supply, it was found that the energy resolution improves up to an APD gain of 500, especially for the lowest photon energies. Only beyond a gain of 600, the performance will worsen compared to the response at gain 500 due to an increased excess noise factor.

Answer for the Backward Endcap:
For the backward endcap calorimeter the expected radiation damage is so low that only small APD gain adjustments will be possibly needed. Anyhow, the high voltage regulation boards are able to provide voltages up to 450 V, which is well above any APD breakdown voltage. Therefore technically, any gain is virtually accessible. The excess noise was estimated by the Gießen group to become relevant starting at gain above 500, more than a factor two higher than the planned gain value. The light yield loss to be compensated, on the other hand is estimated to be at most about 20 %.

4 Mechanical Systems

4.1 Structural

4.1.1 Maximum Stress

Question:
What are the maximum stresses and deflections for the operational conditions for the barrel and endcaps? Please also include seismic and magnet quench loads.

Answer for the Forward Endcap:
The forward endcap ist suspended in an aluminum support frame (Fig. 1). The suspension is realized in a way that allows movement of the detecor in its frame in vertical direction. Such movement is occuring during build up when the backplane carrying the submodules is successively loaded with submodules. Moreover the frame itself is allowed

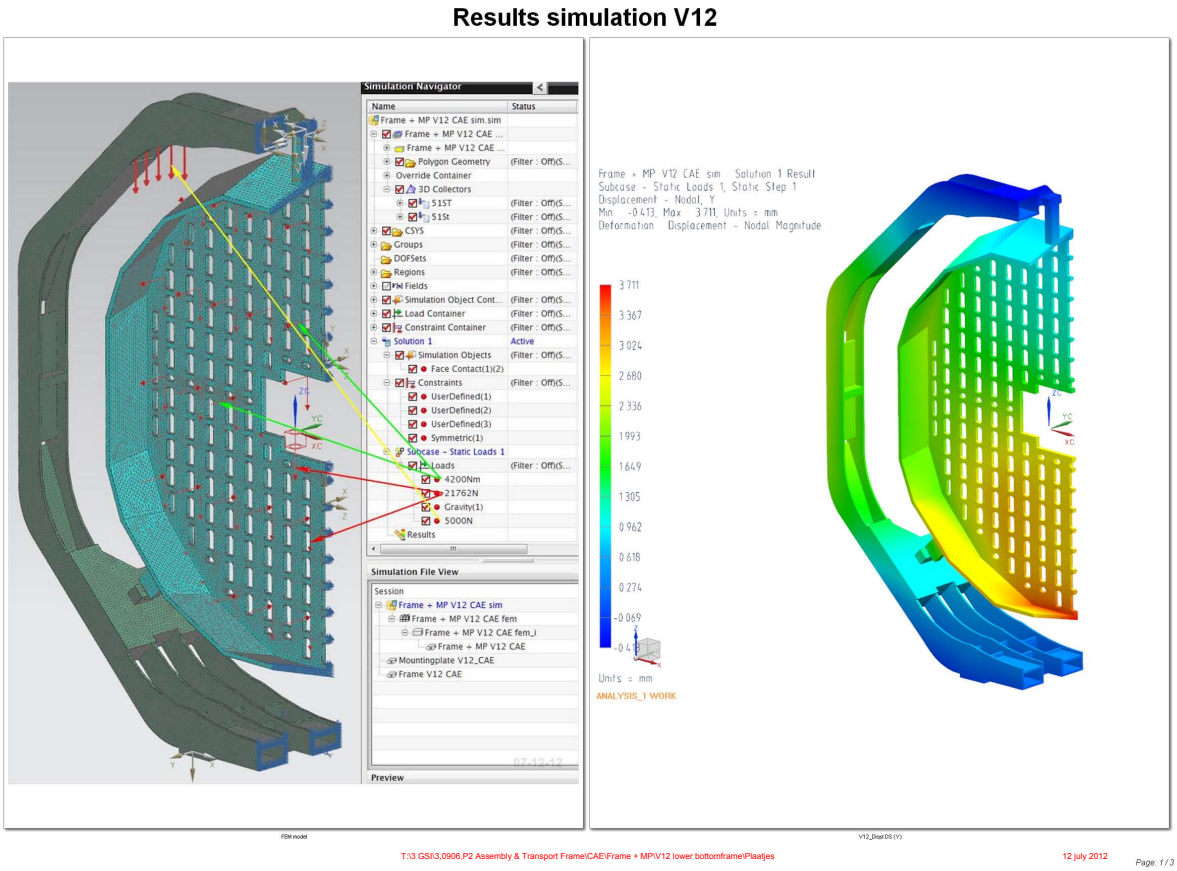

Figure 1: Visualization of FEM calculation of the expeted deformation of the forward endcap support frame.

to bend and taking up seismic loads as expected to occur in Darmstadt if neccessary. Securing elements screwed to the magnet yoke and gearing into cutouts in the left and right upper part of the forward endcap aluminum support frame prevent the forward endcap from tipping and movement in the horizontal direction as expected in cases such as accidental magnet quenches (Fig. 2).

Answer for the Barrel:
The slices of the barrel support each other. On both ends of the barrel, each slice is connected to a stiff support ring. The rings themselves are attached to the surrounding cryostat. There are gaps between the slices and the cryostat, between the crystals from one slice to the other and around each supermodule, which allows movement and deformations. Simulations have been performed applying a three dimensional acceleration vector $\vec{a} = (a_x, a_y, a_z)^T$ with values up to $a_x = 0.3, a_y = 1.3, a_z = 0.3$ in units of g. The main parameters are summarized in Tab. 1. Exemplary visualizations of the deformation can be seen in Fig. 3 and the stress in Fig. 4.

According to the simulations, the maximum allowed deflection of $U_{max} = 2\,mm$ was

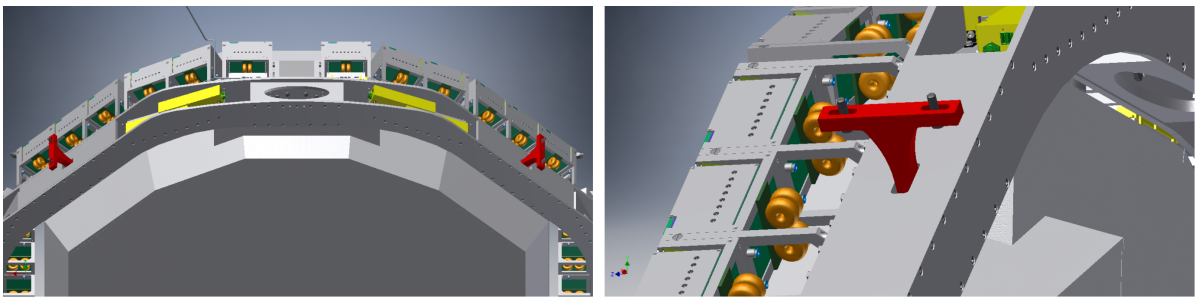

Figure 2: Securing elements (red) screwed to the magnet yoke preventing the forward endcap frame from tipping and movement in the horizontal direction.

Table 1: FE seismic load simulation summary for the barrel. U_{max} is the maximum displacement and S^{eqv}_{max} the maximum stress.

	seismic load vector / g			
	$(0, 1, 0)^T$	$(0.3, 1.3, 0)^T$	$(0, 1.3, 0.3)^T$	$(0.3, 1.3, 0.3)^T$
$\mathbf{U_{max}}$ / mm	0.43	0.56	0.55	0.56
$\mathbf{S^{eqv}_{max}}$ / MPa	59	77	73	74

not exceed. The reference values for the maximum stress of the used materials are the following:

- Stainless Steel (standard steel of type 12X18H10T as used for the barrel's rings) yield streng $\sigma_{0.2} = 210$ MPa and ultimate tensile strenght $\sigma_b = 530$ MPa
- Al Alloy GAL C330R (used for the beams of the barrel) $\sigma_{0.2} = 300$ MPa and $\sigma_b = 350$ MPa

Those values have not been exceeded as well within the simulations. Therefore it is not expected, that seismic events will be a risc for the barrel EMC.

4.1.2 Differences in Expansion Coefficients

Question:
Do the differences in the coefficients of thermal expansion cause increased stresses or is this accounted for in the assembly clearances and tolerances?

Answer:
It is accounted for the thermal expansion and contraction during warm up and cool down. All mechanical structural elements of the cold volume are made from aluminum. The highly modular design of each calorimeter subunit includes in addition gaps between each module. The carbon fibre alveoli suspending the crystals and the aluminum inserts which cover the read-out units and represent the mounting interface to the backplate are proven to perfectly handle the 50 K temperature difference between manufacturing and operation temperature. This was shown during operation of the submodules in the

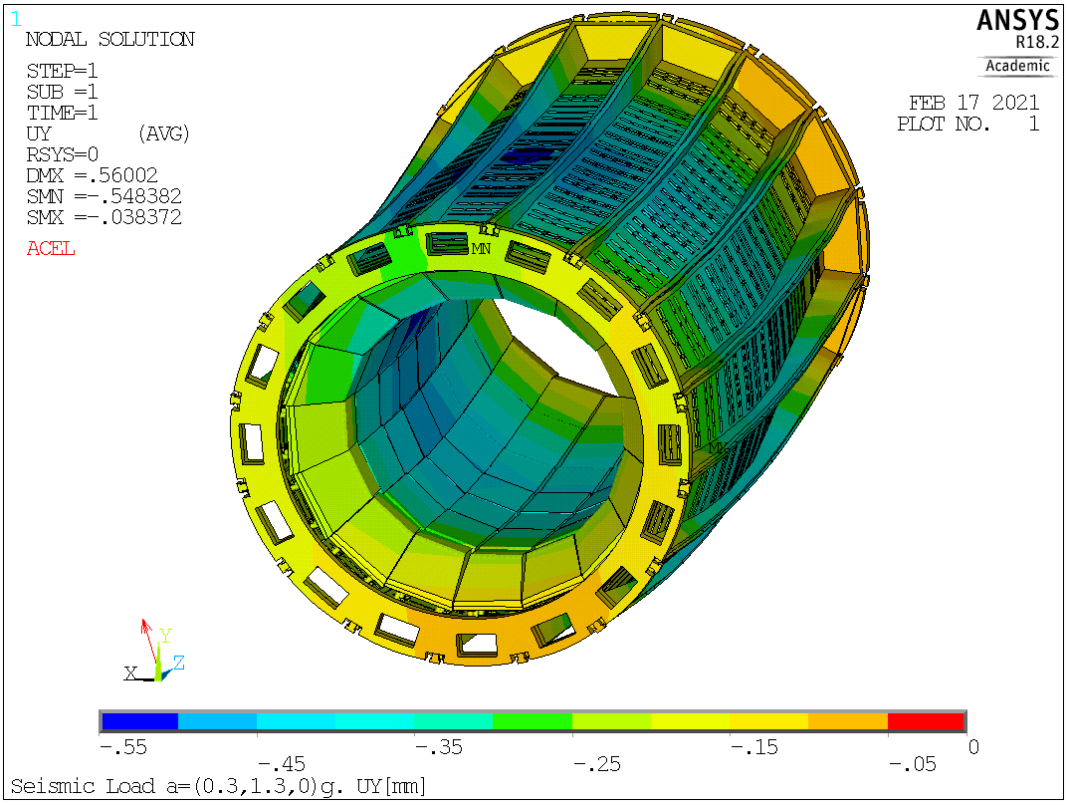

Figure 3: Displacement Field in the Barrel.

test beam prototypes and when cooling down to $\overline{\text{P}}$ANDA operation temperature during precalibration of the submodules in the cosmics test stand.

4.2 Thermal

4.2.1 Cooling/Warming Duration

Question:
How long does it take for the cold region to get to its operating temperature ($-25\,^{\circ}\text{C}$) and return to room temperature?

Answer:
The cooling down and warming up procedures do intentionally use a low temperature gradient to protect the scintillation crystals. Due to the thermal inertia of lead tungstate, changing the temperature too fast will cause a large temperature difference within the crystals which causes mechanical stress. To cool down the crystals from room temperature down to $-25\,^{\circ}\text{C}$ in about 24 h requires a cooling power of 2400 W. The duration of cooling down from $(21.84 \pm 0.31)\,^{\circ}\text{C}$ to $(-25.0 \pm 0.5)\,^{\circ}\text{C}$ (i. e. reaching of a stable temperature) has been determined by means of a prototype for the forward endcap EMC

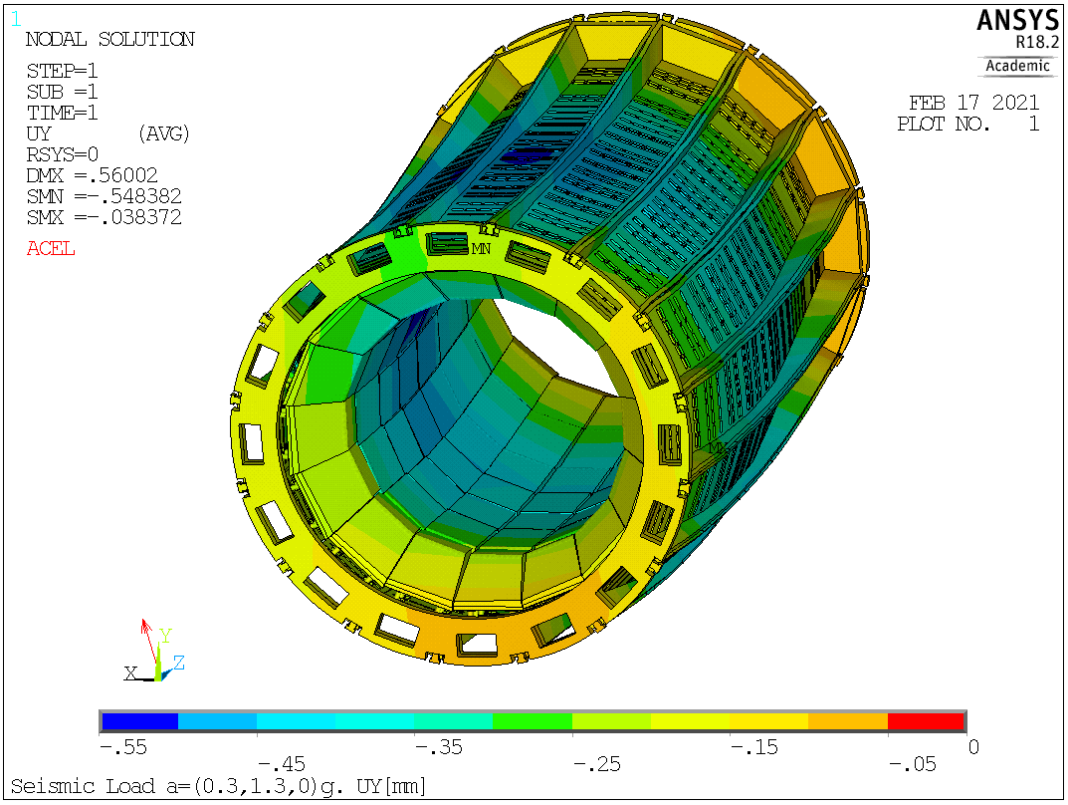

Figure 4: Stress Equivalent in the Beams of the Barrel.

to (28.2 ± 1.5) h. The warm-up time to get from the operating temperature back to ambient temperature takes about the same time.

For the barrel EMC the duration of the heating and cooling towards stable levels has been determined by transient FE analysis. The barrel can be heated up in roughly 25 hours. After $30-41$ hours of cooling, FEA suggests that thermal equilibrium is reached.

Thus we assume less than 2 days for a complete cool down.

4.2.2 Temperature Stability

Question:
What level of control of temperature stability and resolution is required and what do you think you can achieve?

Answer:
Taking into account the temperature dependence of the light yield of the crystals and the gain of the APDs, the time stability of the temperature should stay within 0.1 °C in order for the impact of temperature fluctuations on the energy resolution to stay well below a sensible level. The temperature of the cooling liquid is regulated by electric in-line heating elements to reach the required temperature stability.

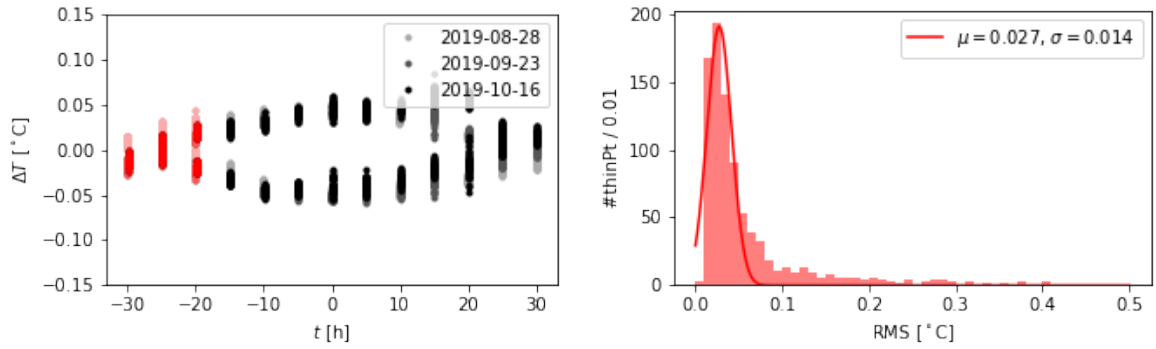

Figure 5: Difference of measurement values and to the mean calibration fit function as a function of temperature with data corresponding to the temperatures −20 °C, −25 °C and −30 °C displayed in red for sensor #1662 (left) and distribution of the RMS values corresponding to these temperatures for sensors which have been calibrated successfully more than once (right).

For the barrel and forward endcap the temperature of the crystals is measured and provided as feedback to the temperature regulator. To measure the temperature of the barrel and forward endcap they will be equipped with flat Pt-100 sensors produced in Bochum. To ensure reproducibility these sensors are calibrated several times before they are validated for usage in the EMC.

Unfortunately, the hysteresis effect cannot be corrected for so that it needs to be included in the uncertainty. The precision of the Pt-100 sensors is estimated to 0.027 °C according to the following approach: The root mean square of all individual datapoints with respect to the mean calibration fit function of all successful calibrations is calculated. The differences between the individual datapoints and the mean calibration fit function are shown exemplary for sensor #1662 in Fig. 5 (left). Since only the precision at −25 °C is relevant, only the datapoints corresponding to the temperatures −20 °C, −25 °C and −30 °C are used. For sensor #1662 this RMS is 0.016 °C. The distribution of the obtained RMS values for all temperature sensors which have been calibrated successfully more than once is fitted with a Gaussian as shown in Fig. 5 (right). The mean of this Gaussian is 0.027 °C. Sensors with an RMS value above $\mu + 3\sigma = 0.07$ °C won't be used.

Although no temperature regulation is foreseen for the backward endcap, a temperature monitoring with flat Pt-100 sensors produced in Mainz, which are placed among the crystals, will be available. The resolution of the measurement has shown to be of the order of or better than 0.1 °C, allowing to detect if the temperature fluctuations exceed the tolerable level. In prototype tests, involving a cooling system similar to the one foreseen for the backward end-cap calorimeter, this level of temperature stability could be maintained for the full duration of the tests, i. e. up to a few days.

According to simulation results, the maximum temperature difference between the extremities of the crystals should not exceed 2 °C, in order to have no effect on the energy resolution. The actual temperature gradient inside the detector can not be measured

until the full system is built and brought into operation. However, FEM simulations of the cooling system planned for the backward calorimeter show maximum temperature differences along the crystals lower than 0.5 °C. The same simulation tools and methods were validated by calculating the temperature distribution for the prototype system, and finding it in agreement with measurements.

4.2.3 Thermal Insulation of the Slices

Question:
How are the sides of a slice thermally insulated from the environment? How are gaps in thermal isolation between slices mitigated?

Answer:
Slices are not thermally insulated from each other. The inner face of the barrel will be insulated by vaccuum insulation panels covering three to four slices. Manufacturing of the panels has advanced since their first application in $\overline{\text{P}}$ANDA prototypes. The goal is to complete the front insulation with the least number of gaps as production, transport and handling allows. Gaps will be mitigated by connecting the VIP faces with flexible insulating glue.

4.2.4 Air Penetration

Question:
How is potential air penetration mitigated?

Answer:
As in the various beam time prototypes for the forward endcap potential air penetration is prevented by flushing the detector volumes with dried and cooled air at a slight overpressure of less than 50 mbar. A safety outlet valve opens in case of excessive overpressure. The cold volume is kept close by thin aluminum plates in the front and back and by gluing the cables in the electronics frame in between.

For the barrel section, a potential air penetration is avoided by controlled provision of dry air with slight overpressure. The inlet of the dry air supply will be located at the upstream interface in vicinity to the service feed-through window and led into the cold section containing the crystals through a duct. In order to avoid leakage through the cable feed-throughs between the crystal section and the thermal insulation layer into the slice support beam (where the back plane electronics boards are located), dedicated rubber fittings will be inserted. Prototypes of these fittings are currently under test with respect to thermal, structural and radiation-tolerance aspects. The supplied dry air will be pre-cooled through a heat exchanger in the chiller devices on the outskirts of the target spectrometer section.

The same mechanism of flushing with dry air is foressen for the backward endcap.

4.2.5 Heat Load

Question:
What is the anticipated additional heat load from the surrounding environment? The TDR indicates 7 W per slice, but what about the endcaps?

Answer:
Just for clarification: The heat load from the surrounding environment is 100 W per slice. The 7 W per slice is only the value for the inner part towards the SciTil/DIRC-detectors.

The total heat load for the forward endcap is approximately 2324 W. Of this, the heat flux, at a temperature difference of 50 K between the surrounding and inside temperatures, is about 264 W due to ambient heat through the insulating panels and the contact adhesive of the panels.

Because the design details of the $\overline{\text{P}}$ANDA inner detectors and their electronic components are not yet fully available, not all heat sources and their positions inside the spectrometer are known by now. Therefore the cooling system of the backward calorimeter was designed in a rather conservative way. The total heat flow entering the detector under an unrealistic worst case scenario of 70 °C outside temperature was estimated around 100 W.

4.2.6 Dew Point

Question:
What is the anticipated dewpoint in the surrounding environment?

Answer:
The conditions in the $\overline{\text{P}}$ANDA hall (beam site) are minimum 20 °C and maximum 26 °C at a minimum relative humidity of 30 % and maximum relative humidity of 40 %, resulting in a dewpoint of 11.5 °C at maximum.